Robotica (2010) volume 28, pp. 47–56. © Cambridge University Press 2009
doi:10.1017/S0263574709005542

Design and control of a haptic interactive motion simulator for virtual entertainment systems

M. Karkoub†,*, M.-G. Her‡ and J.-M. Chen‡

†*Mechanical Engineering Department, The Petroleum Institute, Abu Dhabi, P.O. Box 2533, UAE*
‡*Department of Mechanical Engineering, Tatung University, 40 Chung-Shan North Road, 3rd Sector, Taipei, Taiwan 10451*

(Received in Final Form: March 6, 2009. First published online: April 9, 2009)

SUMMARY

In this paper, an interactive virtual reality motion simulator is designed and analyzed. The main components of the system include a bilateral control interface, networking, a virtual environment, and a motion simulator. The virtual reality entertainment system uses a virtual environment that enables the operator to feel the actual feedback through a haptic interface as well as the distorted motion from the virtual environment just as s/he would in the real environment. The control scheme for the simulator uses the change in velocity and acceleration that the operator imposes on the joystick, the environmental changes imposed on the motion simulator, and the haptic feedback to the operator to maneuver the simulator in the real environment. The stability of the closed-loop system is analyzed based on the Nyquist stability criteria. It is shown that the proposed design for the simulator system works well and the theoretical findings are validated experimentally.

KEYWORDS: Active joystick; Motion simulator system; Virtual entertainment system.

1. Introduction

Virtual reality (VR) systems have become an integral part of many industrial sectors such as aviation, medical, manufacturing (see, for example, [1, 2, 11, 12, 15]). VR systems have been used to train and educate people in the field for economic or other justifiable reasons as in the case of hazardous sites. For example, in-flight simulators have been extensively used to train pilots and would be pilots because human errors could be catastrophic in real situations.[2] In the medical field, VR systems have been used to train doctors to diagnose diseases without intrusive diagnostic procedures.[1,5,12] Most VR systems make use of haptic interfaces which make the operator feel as if s/he is dealing with a physical environment.[13] The interaction between a human operator and machines is achieved through an intermediary device known as "haptic device."[9,14] This device can be programmed to impose arbitrary trajectory-dependent forces on the operator arm. The haptic device has a force feedback characteristic allowing operators to feel the contact on the palm of the hand by grasping a handle or grip. The use and utility of such devices have been on the rise due to the advancements in various technological sectors. The elements of the force feedback mechanism such as connecting rod, linkages, and encoders are mainly passive since neither the controlled object nor the virtual environment provides any force feedback to the operator. However, the haptic device is power actuated and provides a force feedback to the operator. Kazerooni and Her[9] used a haptic interface device for a manpower amplifier. In ref. [9], the authors realized teleoperation for the VR system with haptic characteristics that allows an operator to probe and feel a remote virtual environment.

Haptic devices come in different sizes and shapes; a small pen-based interface arrangement has been used to create free form surfaces[8] or simulate surgical tools. Robot manipulators have been used as the force interface[3,6,10,16]; Hamada *et al.*[4] designed a haptic device that uses a specialized robot manipulator to apply force feedback between the user and the VR environment. Kanai and Takahashi[8] developed a model for a haptic interface device which can give the operator a feel that s/he is maneuvering a mass, or pushing onto a spring or a damper. Minsky and Ouh-Young[15] proposed a dynamic simulator to create virtual textures via a powered joystick system with a force feedback device. Takahashi and Ogata[17] studied the teleoperation and human–machine interfaces and simulated a robotic system using VR technology. In general, robot manipulators have been used by the manufacturing industry for performing certain automation tasks, or used as a joystick/slave-type manipulator in teleoperation. Li and Wang[13] modeled force/torque sensing for a working environment using physical components (e.g. mass and spring/damper) in the VR simulation system. In ref. [7], the operator manipulated a haptic "joystick/slave" telerobotic system through an X–Y Table (joystick) to move a slave robot. The haptic interface used in the experiment helped the operator feel the reaction forces from the slave environment. Building on our previous work,[7] a motion simulator system is designed here to interact with a virtual reality environment represented by a submarine system. The slave robot is replaced with a 2D motion simulator system and the X–Y Table is replaced with a joystick. The system requires controllers to drive the seat of the simulator as well as the haptic interface. The advantage of the control scheme presented in this paper is that the dynamics of the human arm, the actuators, and the environment are included in the closed-loop control model for stability analysis.

* Corresponding author. E-mail: mkarkoub@pi.ac.ae

It is worth mentioning that the motion simulator presented here is merely a platform that can be integrated with many applications. For example, the authors are currently working on integrating the motion simulator with a real-time pipeline inspection system. The motion simulator will be used in conjunction with a pigging system to do real-time inspection of pipelines. The operator will be able to maneuver the pig inside the pipeline and observe reconstructed defects from the data relayed by the pig.

The rest of the paper is organized as follows: the positioning problem of a 1D haptic simulator is designed and analyzed in Section 2. In Section 3, the control synthesis and analysis for the simulator is presented. The virtual reality motion simulator system is analyzed and the corresponding control strategy is presented in Section 4. Finally, some concluding remarks are listed in Section 5.

2. Simulator System Positioning Control problem

In this section, we analyze the performance and control of a one-degree-of-freedom motion simulator system. The findings in this section will be extended to a 2D motion simulator in the following section assuming the simulator motion is slow enough such that coupling between the different directions of motion can be ignored.

The following variables are used throughout the paper:

F_j: Force imposed on the joystick by the human arm.
F_s: Force imposed on the haptic interface device by the environment.
y_j: Position of the joystick.
y_s: Position of the simulator.
v_j: Control input for the actuator of the joystick.
v_s: Control input for the actuator of the simulator.
u_h: Force of the muscle of the human arm.
A_f: Transfer function of the force.
A_y: Transfer function of the position.
S_j: Sensitivity of the human arm force to the position.
S_s: Sensitivity of the environment force to the position.
T_h: Transfer function of the human arm impedance.
T_e: Transfer function of the environment impedance.
A_V: Acceleration of the virtual environment.
A_R: Acceleration of the motion simulator.
α: Gain of the transfer function.
b: Coefficient of friction.
D: Resistance of water.
d: Distance from the applied thrust force to the center of mass.
F: Forward force of the virtual submarine.
F_h: Force of operator's hand.
C_j: Closed-loop controller of the joystick.
C_s: Closed-loop controller of the motion simulator.
K: Proportion (amplifier) between virtual environment and motion simulator.
K_{ej}: Compensator transfer function of the joystick.
K_{es}: Compensator transfer function of the motion simulator.
K_{hs}: Motion simulator transfer function.
m: Mass of the virtual submarine.

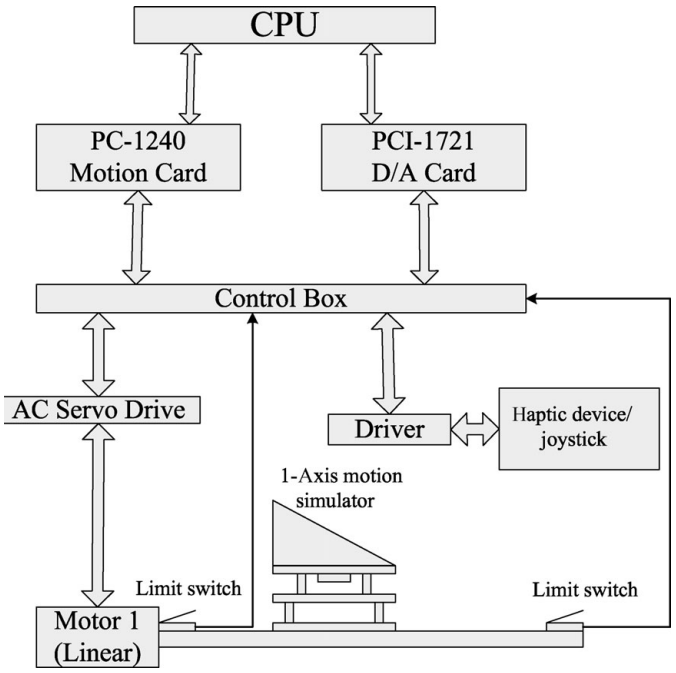

Fig. 1. Hardware connection diagram for the 1-axis motion simulator (no VR environment).

T_{hj}: Force feedback transfer function of the joystick.
T_{hs}: Force feedback transfer function of the motion simulator.
T_{ej}: Transfer function of the virtual environment dynamics of the joystick.
T_{es}: Transfer function of the virtual environment dynamics of the motion simulator.
V: Velocity of the virtual submarine.
X_R, x_R: Displacement of the motion simulator in Laplace and time domains.
x_{limit}: Maximum distance of the motion simulator.
x: Displacement of a virtual submarine.
δ: Angle of the joystick for the virtual submarine.
κ: Coefficient of elasticity.

In the position control problem of the simulator system with unconstrained movements, the nominal operating point of the system can be assumed to be constant. This is so because the contact force between the simulator chair and the environment is dependent on its mass only. However, for constrained movements, such an assumption is no longer valid. The operating point and the system parameters may vary since the environment is unstructured and time varying. In order to model the structure of the simulator system for control purposes for both constrained and unconstrained movements, a general unstructured model is formulated. This model includes the human arm dynamics, handler actuator dynamics, and the environment dynamics. This makes it possible to explicitly derive the stability criterion for the closed-loop system. Figure 1 shows a connection diagram for the hardware of the one-degree-of-freedom simulator system with haptic behavior and the corresponding control block diagram is shown in Fig. 2. Inspecting Fig. 2, the force output of the human arm and the feedback reaction force with haptic

https://doi.org/10.1017/S0263574709005542 Published online by Cambridge University Press

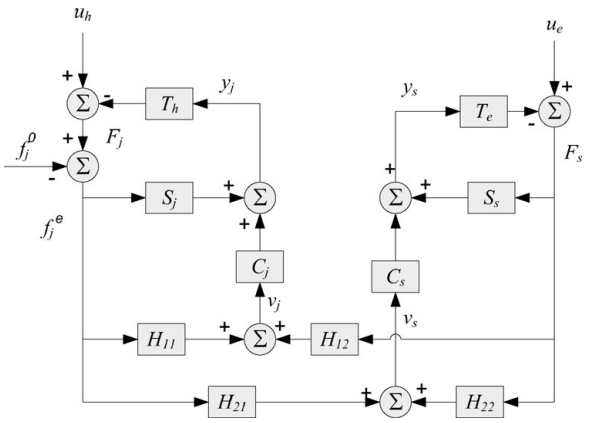

Fig. 2. Control block diagram for the 1-axis motion simulator.

behavior are related as follows:

$$F_{\mathrm{j}} = u_{\mathrm{h}} - T_{\mathrm{h}} y_{\mathrm{j}}, \tag{1}$$

where T_{h} is the transfer function from the joystick handle position to the force and u_{h} is the force supplied by the human muscle.
The position y_{j} of the handle is given by

$$y_{\mathrm{j}} = C_{\mathrm{j}} v_{\mathrm{j}} + S_{\mathrm{j}} F_{\mathrm{j}}. \tag{2}$$

Similarly, on the simulator side, the output force of the seat and the transporting force from the joystick are related as follows:

$$F_{\mathrm{s}} = u_{\mathrm{e}} - T_{\mathrm{e}} y_{\mathrm{s}}, \tag{3}$$

where T_{e} is the transfer function from the seat position y_{s} of the simulator to the feedback force F_{s}.

The actual position of the simulator seat is given by

$$y_{\mathrm{s}} = C_{\mathrm{s}} v_{\mathrm{s}} + S_{\mathrm{s}} F_{\mathrm{s}}. \tag{4}$$

The sensitivity functions S_{j} and S_{s}, in (2) and (4), respectively, map the control forces F_{j} and F_{s}, respectively, to the position of the joystick handle (simulator seat). Whenever the contact force from the joystick handle (environment or loads) is applied to the joystick or the simulator, the hand controller moves if $S_{\mathrm{j}} \neq 0$ ($S_{\mathrm{s}} \neq 0$). If the closed-loop transfer function with a stabilizing controller has a large loop-gain, then S_{j} and S_{s} are negligible compared to C_{j} and C_{s}, respectively. If the handle and the actuators of the haptic interface device are non-back drivable (i.e. system with a geared large transmission ratio), then S_{j} and S_{s} are negligible regardless of the choice of the haptic interface's stabilizing controller. It is worth noting that if the sensitivity functions S_{j} and S_{s} are far away from the operating frequency range, the seat actuator may not drive the seat to the desired position.

3. Controller Design and Stability Analysis

3.1. Controller design

Referring to Fig. 3, C_{j} and C_{s} are the joystick and the seat actuators transfer functions, respectively. S_{j}, S_{s} and H are control parameters to be determined for stability analysis. A large value of H works as a compliant control for the joystick; however, a small value of H stiffens the behavior of the actuator. One cannot arbitrarily choose large values for H because the stability of the closed-loop system may not be guaranteed. Let H be defined as

$$H = \begin{bmatrix} H_{11} & H_{12} \\ H_{21} & H_{22} \end{bmatrix}. \tag{5}$$

Then, the following relationship between the joystick and the simulator can be established:

$$v_{\mathrm{j}} = H_{11} F_{\mathrm{j}} + H_{12} F_{\mathrm{s}} \tag{6}$$

for the joystick and

$$v_{\mathrm{s}} = H_{21} F_{\mathrm{j}} + H_{22} F_{\mathrm{s}} \tag{7}$$

for the simulator.

For the simulator system shown in Fig. 3 with external input signal, the following is obtained:

$$y_{\mathrm{j}} = C_{\mathrm{j}}(H_{11} F_{\mathrm{j}} + H_{12} F_{\mathrm{s}}) + S_{\mathrm{j}} F_{\mathrm{j}}, \tag{8}$$

$$y_{\mathrm{s}} = C_{\mathrm{s}}(H_{21} F_{\mathrm{j}} + H_{22} F_{\mathrm{s}}) + S_{\mathrm{s}} F_{\mathrm{s}}. \tag{9}$$

Let A_{y} be the gain which amplifies the interaction between the position of the joystick and the simulator such that

$$y_{\mathrm{s}} = A_{\mathrm{y}} y_{\mathrm{j}}. \tag{10}$$

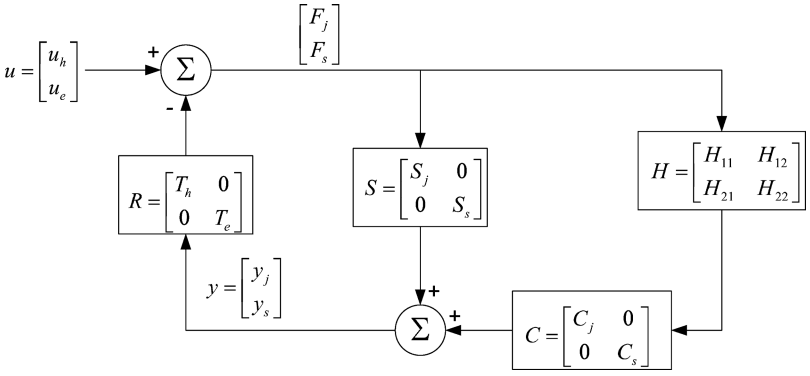

Fig. 3. Simplified control block diagram for the 1-axis motion simulator.

https://doi.org/10.1017/S0263574709005542 Published online by Cambridge University Press

Using (8), (9), and (10) leads to

$$C_s(H_{21}F_j + H_{22}F_s) + S_sF_s = A_y(C_j(H_{11}F_j + H_{12}F_s) + S_jF_j) \tag{11}$$

which leads to

$$C_sH_{21} = A_y(C_jH_{11} + S_j), \tag{12}$$

$$C_sH_{22} + S_s = A_yC_jH_{12}. \tag{13}$$

Equations (10), (12), and (13) show that the haptic behavior can transfer the position of the joystick to that of the simulator and vice versa. Furthermore, let f_j^0 be the human arm output force applied to maneuver the handle of the joystick in the absence of reaction forces from the environment. From Fig. 2, the following relationship is obtained:

$$F_j - f_j^0 = f_j^e. \tag{14}$$

In the absence of reaction forces from the environment ($T_e = 0$ and $f_j^e = 0$), u_e vanishes which leads to

$$y_j = C_jH_{11}f_j^0 + S_jf_j^0. \tag{15}$$

If $T_e \neq 0$ and $u_e = 0$, then

$$y_j = C_j\left(\frac{-H_{12}T_eC_sH_{21}}{1 + T_eC_sH_{22} + S_sT_e} + H_{11}\right)F_j + S_jF_j. \tag{16}$$

If $f_j^e \neq 0$, one can substitute f_j^0 defined in (14) into (15) to obtain

$$y_j = C_jH_{11}\left(F_j - f_j^e\right) + S_j\left(F_j - f_j^e\right). \tag{17}$$

Algebraic manipulation of Eqs. (16) and (17) leads to

$$f_j^e = \frac{-C_{ej}}{C_jH_{11} + S_j}F_j \tag{18}$$

where

$$C_{ej} = \frac{C_jH_{12}T_eC_sH_{21}}{1 + T_eC_sH_{22} + S_sT_e}. \tag{19}$$

A relationship between F_s and F_j can be obtained from Fig. 3 as follows:

$$F_s = \frac{-C_sT_eH_{21}}{1 + T_eC_sH_{22} + S_sT_e}F_j. \tag{20}$$

Using Eqs. (18)–(20), the following relationship is obtained:

$$\frac{F_s}{f_j^e} = \frac{H_{11}C_j + S_j}{H_{12}C_j} =: A_f. \tag{21}$$

If A_f and H_{11} are known, H_{12} can be obtained from (21) as

$$H_{12} = \frac{C_jH_{11} + S_j}{A_fC_j}. \tag{22}$$

Similarly, using Eqs. (12) and (13), H_{21} and H_{22} are given by

$$H_{21} = \frac{A_y(C_jH_{11} + S_j)}{C_s}, \tag{23}$$

$$H_{22} = \frac{(A_y/A_f)(C_jH_{11} + S_j) - S_s}{C_s}. \tag{24}$$

A_f is defined as the ratio of the position imposed on the handle by the human arm to the force imposed on the simulator by the environment. It can be interpreted as the sufficient force to drive the handle actuator of the joystick. It can also be viewed as the ratio that transfers the force f_j^e to the simulator force F_s due to the inertia force from the environment. Hence, the compensator design problem is dependent on the proper selection of H_{11}, H_{12}, H_{21}, and H_{22} for the simulator system.

3.2. *Stability analysis*

From Fig. 3, one can derive the input–output equation of motion such that

$$y = (I + CHR + SR)^{-1}(CH + S)u =: Pu. \tag{25}$$

The transfer matrix P from u to y is stable if it is a proper stable rational matrix and $|I + CHR + SR| \neq 0$. If the compensator H is chosen such that $S + CH$ is approximately constant, then the handle actuator serves as a spring with a nonrigid coupling in response to F_j. However, if $S + CH$ is approximated by a single or double integrator, the handle actuator acts as a damper. It is assumed that H is a stable linear transfer function and the closed-loop system is stable when $H = 0$, which means that the operator and joystick subsystem and the environment and simulator subsystem remain stable when no compensator H is used in the loop. Also, the loop gain SR has the same number of right-hand-side poles (RHP) as $CHR + SR$.

There are two elements in the feedback loop: RS and RHC. RS represents the natural feedback loop resulting from direct reaction between the human arm and the joystick while RCH represents the interaction resulting from the handle actuator of the joystick and the seat actuator of the simulator. Figure 3 shows that when $H = 0$ and C is not there, SR can be considered as the natural loop gain generated by the interaction of the human arm and the tactual interface. In other words, the human operator directly maneuvers the handle with haptic behavior and no force is transferred to the simulator seat actuator. The goal here is to select a compensator H such that the stability of the closed-loop system is guaranteed.

Based on the maximum modulus theorem and the Nyquist stability criterion, when $H = 0$, the net number of encirclements equals the number of zeros of $I + SR$ in the RHP minus the number of open-loop poles of SR in the RHP. When $H \neq 0$, in order to ensure the stability of the closed-loop system, the net number of encirclements should be equal to the number of zeros of $I + CHR + SR$ in RHP minus the number of zeros of $CHR + SR$ in the RHP. Since $CHR + SR$ and SR have the same number of poles in the RHP, the net number of encirclements of SR is equal to that

https://doi.org/10.1017/S0263574709005542 Published online by Cambridge University Press

of $CHR + SR$ and the stability analysis can hold for both cases.

In order to ensure the stability of the closed-loop system, the following conditions must be satisfied:

1. $I + CHR + SR$ is analytic in RHP;
2. $I + CHR + SR$ has a proper stable inverse transfer function.

Condition 2 implies the encirclements of $I + CHR + SR$ do not cross the $j\omega$-axis of the s-plain for all frequency, i.e. $|I + CHR + SR| \neq 0, \forall w \in [0, \infty)$. From the maximum modulus theorem

$$\|I + CHR + SR\| = \sup_{w\in[0,\infty)} |I + CHR + SR|. \quad (26)$$

The norm of $I + CHR + SR$ is the radius of the smallest circle that contains the Nyquist plot of $I + CHR + SR$. Hence, $I + CHR + SR$ has a proper stable inverse transfer function *if and only if* $I + CHR + SR$ has no zeros in the RHP or,

$$\inf_{w\in[0,\infty)} \|I + CHR + SR\| > 0. \quad (27)$$

In other words, $I + CHR + SR$ has a proper stable inverse transfer function whenever

$$|CHR + SR| < 1 \ \ \forall w \in [0, \infty). \quad (28)$$

Using Fig. 3 and Eqs. (12), (13), and (22), the following is obtained:

$$\begin{aligned} &|I + CHR + SR| \\ &\quad = T_h T_e[(C_j H_{11} + C_j)(C_s H_{22} + S_s) - C_j C_s H_{12} H_{21}] \\ &\qquad + (C_s H_{22} + S_s) T_e + T_h (C_j H_{11} + S_j) + 1 \\ &\quad = C_j H_{11} (T_e \frac{A_y}{A_f} + T_h) + S_j (T_e \frac{A_y}{A_f} + T_h) + 1. \end{aligned} \quad (29)$$

From Eq. (28)

$$|C_j H_{11}| < \left| S_j + \frac{1}{(A_y/A_f)T_e + T_h} \right|, \forall w \in [0, \infty). \quad (30)$$

Therefore, if stability criterion (30) is satisfied, then the closed-loop system is stable. By proper selection of H_{11}, the stability margin of the system can be obtained if A_y, A_f, T_e, and T_h on the right-hand side of inequality (30) are known *a priori*. It is worth noting that if H_{11} in (30) is large, the stability margin of the system will be small, and the system will be less stable. Also, if S_j is small, this implies a corresponding small value for H_{11}, i.e. the larger the transmission of the mechanism gets, the smaller the range gets for the value of H_{11}. Moreover, when S_j approaches zero, i.e. a non-back-drivable case, then the size of $|C_j H_{11}|$ is restricted by $|1/(\frac{A_y}{A_f} T_e + T_h)|$ to a small range.

In the constrained environment, the parameter T_e will be used to satisfy the stability condition. The stability condition can then be obtained by rewriting stability criterion (28) as follows:

$$\left| \frac{A_f}{A_y} \left(S_s + \frac{1}{C_j H_{11} + S_j} \right) \right| > |T_e|, \quad \forall w \in [0, \infty). \quad (31)$$

Note that the left-hand side of inequality (31) is equal to F_j/y_j. When the system satisfies inequality (30) and H_{11} is fixed, the value of the environment parameter T_e becomes smaller than the left-hand side of inequality (30). This prevents the value of T_e from exceeding the value of F_j/y_j.

4. Analysis of the VR Motion Simulator System

A 1-axis and 2-axis simulators have been built in our laboratory. The first simulator was used to test the haptic interface and the interaction between the VR system and the simulator (see Figs. 4 and 5). The difference between the 1-axis and 2-axis systems is a rotation actuator added at the bottom of the simulator seat. The VR system is the same for both simulators which is a submarine system. However, in the 1-axis case, the submarine is limited to rectilinear motion whereas in the 2-axis case, the submarine is allowed to move in the plane. The main components of the simulator are listed in Table I and the connection diagram is shown in Fig. 6. The simulator system includes the motion simulator and joystick/haptic interface device, and the VR system (force feedback joystick and image/sound system). The simulator seat is confined to move in a limited space; however, the virtual environment is not. In order to simulate the unlimited space in the virtual environment, some sort of mapping has to occur. This can be done through a filter to determine the boundaries of the simulator seat and confine the seat motion to those boundaries. Due to the difference in the actual working area of the simulator seat and the virtual environment, three scenarios present themselves: real space and virtual space are the same, real space and virtual space are α-fold of each other, and limited real space and unlimited virtual space. Let us assume that the proportion of virtual space and reality space is K. Given the fact that the virtual space is unlimited and the reality space is limited (maximum length of the motion simulator), one could obtain a range of values for K which optimize the response of the system with respect to the operator experience.

The variation of the virtual system is sensed through vision which is in direct link with the motion of the simulator (see Fig. 7). The acceleration and displacement in the virtual environment are observed in true magnitude (1 to 1 ratio); however, the motion of the simulator is sensed as a scaled quantity (1 to K ratio) and in phase with the virtual environment. The diagram of the multiple bilateral control system is shown in Fig. 8. The operator is able to feel the force feedback from the joystick and the motion simulator through the transfer functions T_{hj} and T_{hs}, respectively. The transfer functions C_s and C_j represent the closed-loop controllers for the simulator and joystick, respectively. The environment dynamics is represented by the transfer functions T_{ej} and T_{es} whereas K_{ej} and K_{es} are the compensator transfer function for the joystick and simulator forces F_j and F_s. The transfer functions T_{ej}, T_{es}, K_{ej}, and K_{es} provide vision feedback to the operator. Clearly, there are two interacting systems in the

https://doi.org/10.1017/S0263574709005542 Published online by Cambridge University Press

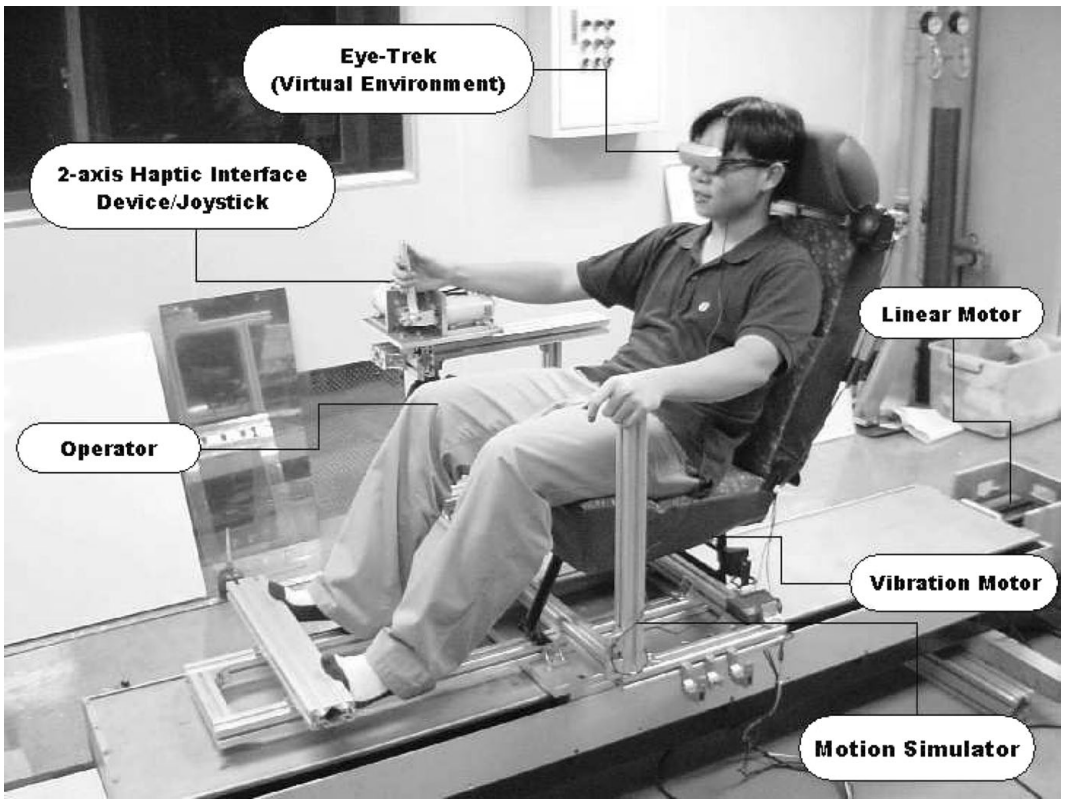

Fig. 4. Photo of the 1-axis motion simulator with VR environment.

closed-loop diagram for the output y_j of the joystick and y_s for the simulator. The overall closed-loop model includes a bilateral control interface between two haptic devices and a virtual environment.

When the joystick is manipulated, the operator feels a force feedback from the joystick, motion feeling from the motion simulator, and vision from the virtual environment. At the same time, the velocity data of the joystick is sent to the virtual environment. Therefore, the motion simulator will move according to the dynamics of the transfer function $K_{hs} = Ks/(s + a)$ (see Fig. 9). It is worth noting that, if the motion simulator moves abruptly, it will cause the joystick to vibrate. However, it is assumed here that the vibration of the joystick is absorbed by the operator hand. Therefore, one needs to adjust the gain K such that the noise from the motion simulator does not get transmitted to the joystick to avoid instability.

4.1. Control analysis

4.1.1. Acceleration of the virtual environment and motion simulator. First, we develop a relationship between the acceleration of the virtual environment and the motion

Table 1. Simulator equipment list.

Item	Qty.	Description
PC	1	Intel P4-2G, RAM DDR 1G, 3D Graphics Card 128Mb
PCI-1240 Motion card	1	Advantech, 4-axis Universal PCI Stepping/Pulse-type Servo Motor Motion Control Card
PCI-1721 D/A card	1	Advantech 12-bit, 4-channel Advanced Analog Output Card, 10 MHz maximum digital update rate
TV box	1	LKV 2000 WinMPG Video Convert VGA TO AV
Control box	1	Control box designed in our lab, I/O, and motor drives
Joystick	1	Logitech joystick, Extreme 3D Pro.
Eye trek	1	Olympus Eye-Trek FMD-200
AC servo drive	1	Sinano, 3MC30ZE-3DGEA, 220-V servo motor drive
AC servo motor	1	DELTA ASMT04L250AK, 400 W, 2500 PPR 3000 RPM, 1.27 Nm
DC Servo motors	2	Sinano servo motor
DC Servo motors	1	Panasonic DC motor
2-axis haptic interface	1	Mechanism designed in our lab
Encoder	1	Sinano, resolution 120,000 pulse/rev

https://doi.org/10.1017/S0263574709005542 Published online by Cambridge University Press

Fig. 5. Photo of the 2-axis motion simulator with VR environment.

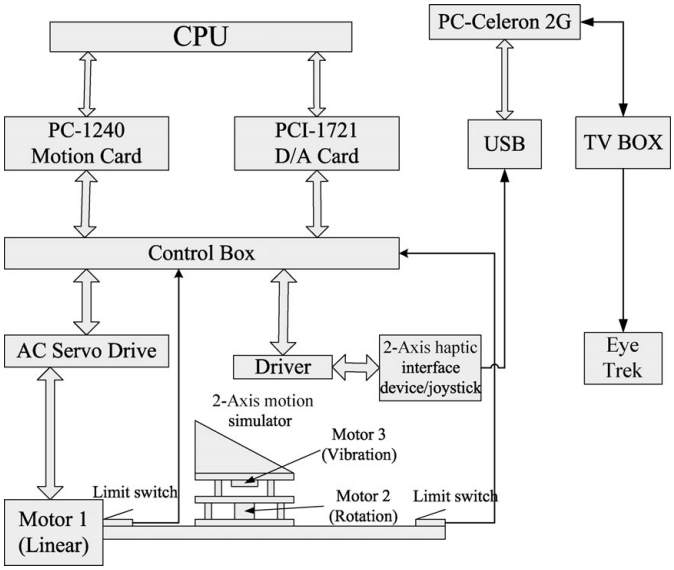

Fig. 6. Hardware connection diagram for the 2-axis motion simulator.

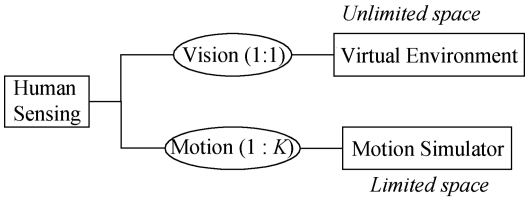

Fig. 7. Interaction flow diagram of the motion simulator.

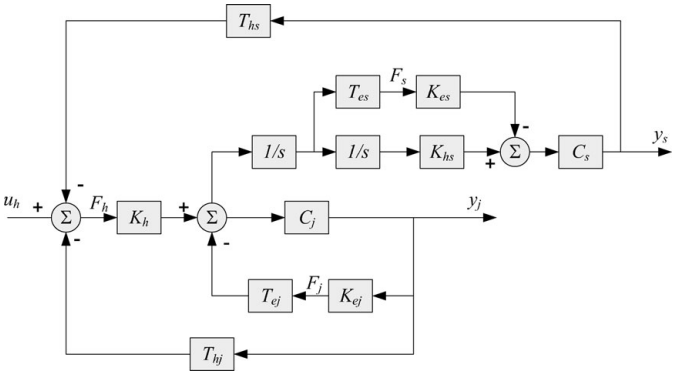

Fig. 8. Control block diagram for the 2-axis motion simulator with VR environment.

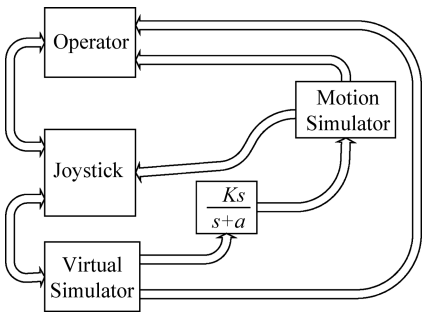

Fig. 9. Flow diagram of the motion simulator.

simulator. In this simulator design, it is assumed that the joystick motion represents the velocity of the virtual reality environment. The transfer function between the motion simulator and the virtual environment is assumed to be of the form $Ks/(s+a)$ which is basically a filter. Therefore, if one increases the speed gradually that means the joystick moves slowly. In other words, low-frequency motion makes the transfer function $Ks/(s+a)$ approach zero. In this case, the seat of the motion simulator will remain fixed and the operator will sense the speed through sight from the virtual environment. However, if we increase the speed very quickly, which means the joystick moves very fast, the output of the transfer function $Ks/(s+a)$ approaches K. That means there is a K-fold relationship between the motion simulator and the virtual environment.

Let V and A_v denote the velocity and acceleration of the virtual environment, respectively. Therefore,

$$A_v = sV$$

https://doi.org/10.1017/S0263574709005542 Published online by Cambridge University Press

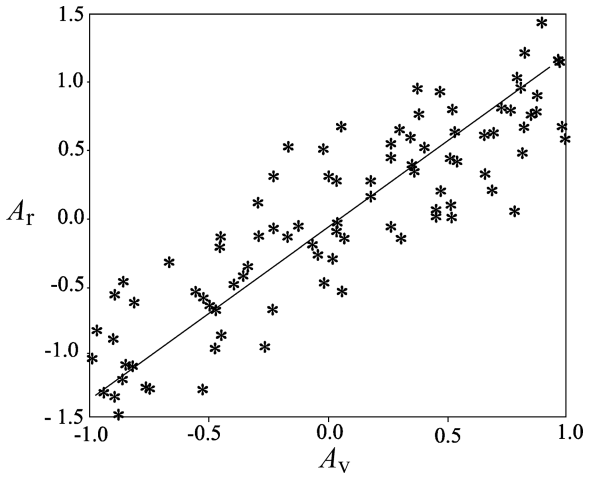

Fig. 10. Experimental relationship between simulator and VR environment accelerations.

assuming zero initial conditions. Now, if we denote by A_R and X_R the acceleration and the displacement of the motion simulator, respectively, we can write

$$X_R = \frac{K}{s+a}V$$

and

$$A_R = s^2 X_R = \frac{Ks^2}{s+a}V.$$

Thus, the ratio of the motion simulator and the virtual environment is calculated as

$$\frac{A_R}{A_V} = \frac{Ks}{s+a}.$$

Therefore, in the case of high frequency, the ratio $\frac{A_R}{A_V}$ approaches K-folds as the joystick moves. However, for low frequency, $\frac{A_R}{A_V}$ approaches zero. Therefore, the operator will sense the acceleration through vision. From Fig. 10, one can see that the ratio $\frac{A_R}{A_V}$ exhibits a proportional distribution. It is worth mentioning that the bode plots of the transfer function $\frac{A_R}{A_V}$ show that the magnitude approaches one and the phase approaches zero at high frequency; and no matter how much the operator accelerates or decelerates, the motion simulator will be in phase with the motion of the virtual environment. That is, when the operator accelerates forward with the joystick, the motion simulator will not reverse direction.

4.1.2. Displacement of virtual environment and motion simulator. As in the previous section, the joystick's displacement is set to the velocity of the virtual environment. This velocity is then integrated to obtain the corresponding displacement of the virtual environment. The displacement of the motion simulator can be obtained through the filter transfer function $Ks/(s+a)$.

$$X_R = \frac{K}{s+a}V$$

where $V = V_{\max}$. Therefore,

$$X_R = \lim_{s\to 0}\frac{K}{s+a}V_{\max} = \frac{KV_{\max}}{a}.$$

Since we already know the maximum displacement of the motion simulator as well as its maximum speed, one can easily determine the value of the gain K.

4.2. The virtual environment

The motion simulator system was used in conjunction with a submarine virtual environment. First, we examine the case when the simulator motion is restricted to one direction.

The free-body diagram of the submarine system is shown in Fig. 11. The equation of motion of the system is given by

$$m\ddot{x} + b\dot{x} = f(t). \tag{32}$$

If the throttle is set to accelerate, such that

$$f(t) = \kappa\delta(t).$$

Then, the transfer function from the throttle force $F(s)$ to the displacement of the submarine $X(s)$ can be written as

$$\frac{X(s)}{F(s)} = \frac{1}{ms^2+bs} \quad \text{or} \quad \frac{X(s)}{\Delta(s)} = \frac{\kappa}{ms^2+bs}, \tag{33}$$

where $\Delta(s)$ is Laplace transform of $\delta(t)$. Therefore, one can derive two system equations that relate the displacement and velocity of the submarine such that

$$X(s) = \frac{\kappa}{ms^2+bs}\Delta(s) \quad \text{and} \quad V(s) = \frac{\kappa}{ms+b}\Delta(s). \tag{34}$$

Let $\delta(t)$ be a step function; therefore, $\Delta(s) = v/s$. One can get the time domain expressions for the displacement and the velocity of the submarine using inverse Laplace such that

$$x(t) = \mathcal{L}^{-1}\left(\frac{\kappa}{ms^2+bs}\frac{v}{s}\right) \quad \text{and} \quad v(t) = \mathcal{L}^{-1}\left(\frac{\kappa}{ms+b}\frac{v}{s}\right) \tag{35}$$

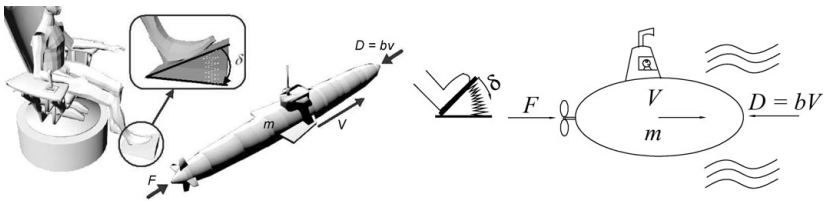

Fig. 11. 1D Virtual reality submarine environment free-body diagram.

https://doi.org/10.1017/S0263574709005542 Published online by Cambridge University Press

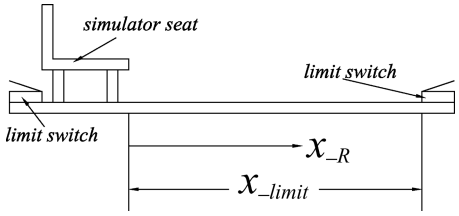

Fig. 12. Schematic diagram of the motion simulator limits.

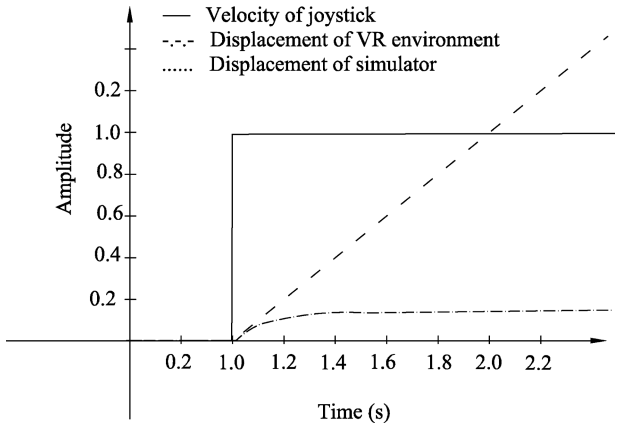

Fig. 13. Time response of the motion simulator VR system.

Therefore, when $t \to \infty$, $x(t) \to \infty$ and $v(t) \to \frac{\kappa v}{b}$ which is the maximum velocity. Moreover, since

$$X_R(s) = \frac{Ks}{s+a}X$$

where K is a scaling factor, $X_R(s)$ can be written as follows:

$$X_R(s) = \frac{Ks}{s+a} \times \frac{\kappa}{ms^2+bs} \times \frac{v}{s} = \frac{\kappa K v}{s(s+a)(ms+b)}.$$

Therefore, the maximum displacement can be found such that

$$x_{\text{Rmax}} = \frac{\kappa K v_{\max}}{ab}.$$

Because of the length limit of the motion simulator (see Fig. 12), x_{Rmax} must be less than x_{limit}. Therefore,

$$\frac{\kappa K v_{\max}}{ab} < x_{\text{limit}} \quad \Rightarrow \quad K < \frac{abx_{\text{limit}}}{\kappa v_{\max}}.$$

Therefore, when $K \approx 1$, the operator's experience will be 1:1 between the real displacement and the virtual displacement. The time response of the VR environment as well as the motion simulator due to a joystick command is shown in Fig. 13. It is clear from the figure that the differences between the working space of the simulator and the VR environment are reflected in the steady-state values of each response. The experimental displacement and acceleration of the simulator in response to the joystick command angle illustrated in Fig. 14 is shown in Fig. 15.

The results of this analysis can be extended to planar motion of the submarine assuming there is no coupling

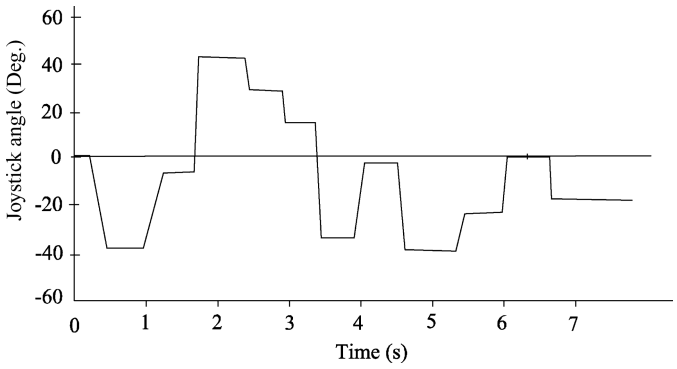

Fig. 14. Joystick command input angle to the simulator.

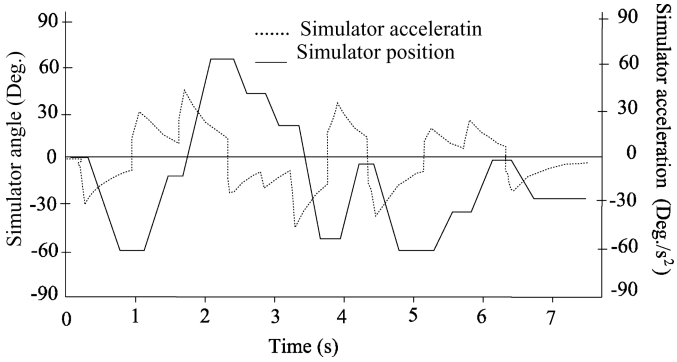

Fig. 15. Position and acceleration of the motion simulator in response to the joystick command angle illustrated in Fig. 14.

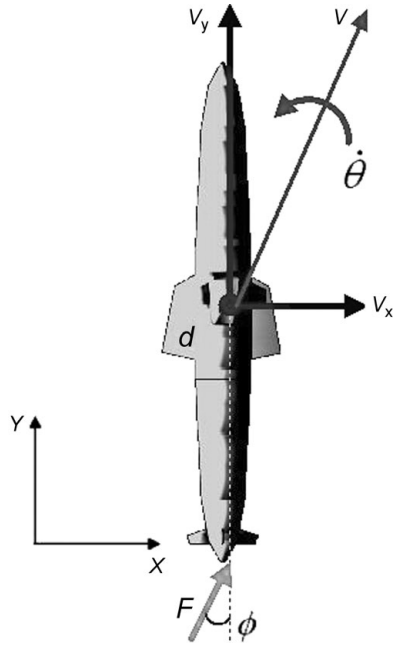

Fig. 16. Free-body diagram of the 2D VR submarine system.

between the x- and y-directions. From Fig. 16, one can write the following equations of motion:

$$\begin{aligned} m\ddot{x} &= F_x - b_x\dot{x}, \\ m\ddot{y} &= F_y - b_y\dot{y}, \\ I\ddot{\theta} &= F_x d - b_\theta\dot{\theta}. \end{aligned} \tag{36}$$

https://doi.org/10.1017/S0263574709005542 Published online by Cambridge University Press

Let us assume that the angle of rotation of the joystick is θ_j and K_j is the corresponding gain. Therefore, the angle ϕ of the submarine is such that

$$\phi = K_j \theta_j \tag{37}$$

Therefore,

$$F_x = F \sin(\phi) \quad \text{and} \quad F_y = F \cos(\phi). \tag{38}$$

Equation (36) can be easily solved and the corresponding x- and y-displacements can be obtained. (Videos from our experiment are posted at http://www.youtube.com/v/Cb1hAbxEnXs for the 1-axis motion and http://www.youtube.com/v/tV3CKfk8y4U for the planar motion.)

Remark 1. The simulator system was also used with a virtual train system and the results were good. The only problem that the operator felt is a little distortion when the train turns a corner or when it stops and goes back straight. However, this problem has been lessened by fine tuning of the yaw control action. It is worth noting that the best results were obtained when the virtual environment was moving at a relatively slow speed.

Remark 2. Although we gained experience from the work presented in ref. [7], we encountered application-specific problems. For example, when a land vehicle is used as the virtual environment, such as a train, the operator does not get a real feel of navigation when the virtual environment moves at a constant speed. A vibration motor underneath the simulator seat is used to improve the experience. However, the vibration motor was not necessary for the submarine virtual environment since sensing is mainly done through vision.

5. Concluding Remarks

A haptic motion simulator is designed for virtual reality applications. The first system is designed assuming linear motion in the x-direction only. A dynamic model for the 1D simulator system with haptic behavior which includes the dynamics of the human arm and the environment is presented in this paper. A sufficient stability criterion based on the maximum modulus theorem and the Nyquist criterion is proposed to guarantee not only the stability of the closed-loop control system but also the performance of the haptic behavior. It was shown that the stability and the desired performance of the closed-loop control system are achievable through a simple filter transfer function. The theoretical and experimental findings were extended to a two-degree-of-freedom simulator assuming the degrees of freedom are independent. The motion simulator system was used with a submarine virtual environment and the results were very satisfactory.

References

1. C. Basdogan, M. Sedef, M. Harders and S. Wesarg, "VR-based simulators for training in minimally invasive surgery," *IEEE Comp. Graph. Appl.* **27**(2), 54–66 (2007).
2. D. K. Boman, "International survey: Virtual-environment research," *IEEE Comp.* **28**, 57–65 (1995).
3. S. E. Everett and R. V. Dubey, "Human–Machine Cooperative Telerobotics Using Uncertain Sensor or Model Data," *Proceedings of the 1998 IEEE International Conference on Robotics and Automation*, Leuven, Belgium (1998) pp. 1615–1622.
4. T. Hamada, K. Kamejima and I. Takeuchi, "Image based operation; A human–robot interaction architecture for intelligent manufacturing," *Proceedings of IECON* (1989) pp. 556–561.
5. S. Haque and S. Srinivasan, "A meta-analysis of the training effectiveness of virtual reality surgical simulators," *IEEE Trans. Info. Technol. Biomed.* **10**(1), 51–58 (2006).
6. B. Hannaford, "Design framework for teleoperators with kinesthetic feedback," *IEEE Trans. Rob. Automat.* **5**(4), 426–434 (1989).
7. M.-G. Her, M. A. Karkoub and K.-S. Hsu, "Design and control of a 2-D telerobotic system with haptic interface," *IMechE J. Syst. Control Eng.* **217**(3), 169–185 (2003).
8. S. Kanai and H. Takahashi, "Modeling and NC Programming for Free-Form Surfaces by Haptic Interfaces," *The 1996 ASME Design Engineering Technical Conference and Conference and Computer in Engineering Conference*, Irvine, CA (Aug. 18–22, 1996).
9. H. Kazerooni and M.-G. Her, "The dynamics and control of a haptic interface device," *IEEE Trans. Rob. Automat.* **10**(4), 453–464 (1994).
10. H. Kazerooni and C. L. Moore, "An approach to telerobotic manipulations," *J. Dyn. Syst. Meas. Control* **119**, 431–436 (1997).
11. V. S. Kuleshov and N. A. Lakota, *Remotely Controlled Robots and Manipulators* (Mir Publishers, Moscow, 1988).
12. D. S. Kwon, K. Y. Woo and H. S. Cho, "Haptic Control of the Master Hand Controller for a Microsurgical Telerobot System," *Proceedings of the 1999 IEEE International Conference on Robotics and Automation*, Detroit, Michigan (1999) pp. 2982–2987.
13. Y. F. Li and J. G. Wang, "Incorporating Sensing in Virtual Environment for Robotic Tasks," *IEEE Instrumentation and Measurement Technology Conference,* St. Paul, USA (May 18–21, 1998).
14. N. Magnenat-Thalmann and U. Bonanni, "Haptics in virtual reality and multimedia," *IEEE Multimedia* **13**(3), 6–11 (2006).
15. M. Minsky and M. Ouh-young, "Feeling and seeing: Issues in force display," *Comp. Graph.* **24**(2), 235–243 (1990).
16. T. Sato, J. Ichikawa, M. Mitsuishi, H. Miyazaki and Y. Hatamura, "Micro-teleoperation with manual task execution posture," *IEEE Control Syst.* **15**(1), 22–28 (1995).
17. T. Takahashi and H. Ogata, "Generating and replanning robot commands based on human operation," *J. JSAI* **8**(4), 448–455 (1994).

https://doi.org/10.1017/S0263574709005542 Published online by Cambridge University Press